Cancer Research

# Characterization of Chemokines and Adhesion Molecules Associated with T cell Presence in Tertiary Lymphoid Structures in Human Lung Cancer

Luc de Chaisemartin[1,2,3], Jérémy Goc[1,2,3], Diane Damotte[1,2,3,4], Pierre Validire[1,6], Pierre Magdeleinat[5,7], Marco Alifano[5], Isabelle Cremer[1,2,3], Wolf-Herman Fridman[1,2,3,8], Catherine Sautès-Fridman[1,2,3], and Marie-Caroline Dieu-Nosjean[1,2,3]

## Abstract

*De novo* formation of tertiary lymphoid structures (TLS) has been described in lung cancers. Intratumoral TLS seem to be functional and are associated with a long-term survival for lung cancer patients, suggesting that they represent an activation site for tumor-specific T cells. Here, we characterized T-cell recruitment to TLS in human lung cancer to identify the adhesion molecules and chemoattractants orchestrating this migration. We found that most TLS T cells were CD62L+ and mainly of CD4+ memory phenotype, but naive T cells were highly enriched in these structures as compared with the rest of the tumor. A specific gene expression signature associated with T cell presence was identified in TLS, which included chemokines (CCL19, CCL21, CXCL13, CCL17, CCL22, and IL16), adhesion molecules (ICAM-2, ICAM-3, VCAM-1, and MAdCAM-1) and integrins (alphaL, alpha4, and alphaD). The presence of the corresponding receptors on TLS T cells was confirmed. Intratumoral PNAd+ high endothelial venules also were exclusively associated with TLS and colocalized with CD62L+ lymphocytes. Together, these data bring new insights into the T-cell recruitment to intratumoral TLS and suggest that blood T cell enter into TLS via high endothelial venules, which represent a new gateway for T cells to the tumor. Findings identify the molecules that mediate migration of tumor-specific T cells into TLS where T cell priming occurs, suggesting new strategies to enhance the efficacy of cancer immunotherapies. *Cancer Res; 71(20); 6391–9. ©2011 AACR.*

## Introduction

The tumor microenvironment is a complex network of different cell types which include cells of the immune system, interspersed with blood and lymphatic vessels. A large body of evidence shows that the local density of tumor-infiltrating T cells influences the clinical outcome of the patients (1, 2). The presence of such cells in the tumor microenvironment prompts the question of where and how these T cells are recruited and activated.

**Authors' Affiliations:** [1]Laboratory "Immunological Microenvironment and Tumors", INSERM U872, Cordeliers Research Centre; [2]University Pierre and Marie Curie, UMRS 872; [3]University Paris Descartes, UMRS 872; Departments of [4]Pathology and [5]General Surgery, Hotel Dieu Hospital, AP-HP; Departments of [6]Pathology and [7]Thoracic Surgery, Institut Mutualiste Montsouris; and [8]Department of Immunology, European Georges Pompidou Hospital, AP-HP, Paris, France

**Note:** Supplementary data for this article are available at Cancer Research Online (http://cancerres.aacrjournals.org/).

L. de Chaisemartin and J. Goc contributed equally to this work.

**Corresponding Author:** Marie-Caroline Dieu-Nosjean, INSERM UMRS872, Cordeliers Research Center, 15, rue de l'école de Médecine, F-75270 Paris cedex 06, France. Phone: 33-1-44-27-90-86; Fax: 33-1-40-51-04-20; E-mail: mc.dieu-nosjean@crc.jussieu.fr

**doi:** 10.1158/0008-5472.CAN-11-0952



Transendothelial migration of lymphocytes to tissues is dependent on a molecular signaling interplay between endocytes and lymphocytes (3). Indeed, recruitment of blood T cells in lymph nodes is well characterized and depends on a specific set of adhesion molecules including CD62L and the chemokines CCL19-CCL21 (T-cell zone) and CXCL13 (B cell follicles), together with their receptors, CCR7 and CXCR5, respectively (reviewed in references 4 and 5). Blood and lymphatic vessels are present in the tumor microenvironment, however, the molecules which orchestrate T-cell entry and trafficking in human cancer are still poorly defined.

We have reported the presence of tertiary lymphoid structures (TLS) in the tumor stroma in non–small cell lung cancer (NSCLC; ref. 6). These structures have been described in many human pathologies, such as autoimmune diseases, infections, or rejection of organ transplants (7–9). They are immunologically functional and have been linked to the local development of cellular and humoral immune responses, using mouse models (10, 11).

In lung cancers, the intratumoral TLS exhibit functional features with clusters of mature dendritic cells (DC) and T cells adjacent to B-cell follicles, which contain proliferating germinal centers (6). As they resemble BALT (Bronchus-associated lymphoid tissues) and were not found in nontumoral tissues, these follicles were termed Ti-BALT, for Tumor-induced BALT. We showed for the first time a long-term

survival in patients with a high density of Ti-BALT (6), suggesting that these structures could be a site of induction of antitumoral responses. The good prognostic value of both Ti-BALT and T-cell densities (1) in cancer patients prompted us to investigate the role of Ti-BALT in T-cell recruitment. Using combined laser microdissection, quantitative PCR (qPCR), immunohistochemistry, and flow cytometry, we identify a set of integrins, adhesion molecules, and chemokines expressed in Ti-BALT and associated with T lymphocyte presence. These data give new insights into T-cell recruitment into cancer TLS that help to understand their organization and prognostic value.

## Materials and Methods

### Patients

Fresh, frozen, and paraffin-embedded lung tumor samples were obtained from lung cancer patients undergoing surgery at Institut Mutualiste Montsouris and Hotel-Dieu Hospital (Paris, France). The main clinical and pathologic features of the patients are presented in the Supplementary Appendix Table SA1. The protocol was approved by local ethic and human investigations committee (n° 2008–133) and by the Assistance Publique-Hopitaux de Paris (AP-HP), in application with the article L.1121-1 of French law. A written informed consent was obtained from the patients prior to inclusion in the study.

### Immunohistochemistry and immunofluorescence

Serial 5-μm tissue sections of paraffin-embedded lung tumors were deparaffinized, rehydrated, and pretreated in appropriate buffer for antigen retrieval (see Supplementary Appendix Table SA2). Then, the sections were incubated with 5% human serum for 30 minutes before adding the appropriate antibodies or isotype controls (see Supplementary Appendix Table SA2). Enzymatic activity was revealed as described previously (6). When necessary, sections were counterstained with hematoxylin. Images were acquired using a Nikon Eclipse 80i microscope (Nikon) operated with Nikon NIS Elements BR software. Immunofluorescent staining was read on a Zeiss LSM 700 confocal microscope with the Zen software (Zeiss).

### Enrichment of tumor-infiltrating lymphocytes

Fresh lung tumor specimens were mechanically dissociated and incubated in a nonenzymatic solution (Cell Recovery solution; BD Biosciences) for 1 hour at 4°C. The cell suspension was then filtrated through a 70-μm filter (BD Biosciences), and the mononuclear cells were isolated by centrifugation over Ficoll Hypaque.

### Flow cytometry

Multiple stainings were done using antibodies against chemokine receptors, anti-CD3 anti-CD4, anti-CD8, anti-CD45RA, anti-CD45RO, and anti-CD62L (see Supplementary Appendix Table SA2). Briefly, after saturation with 2% human serum, mononuclear cells were incubated with the primary antibodies or appropriate isotype controls for 30 minutes at +4°C in the dark. Then, cells were washed and fixed in 1% formaldehyde before the analysis on a LSRII cytometer (BD Biosciences). Flow cytometry data were analyzed with the Diva software (BD Biosciences).

### Laser microdissection

Tumor sections of 14 μm were cut at −20°C and mounted on PEN slide (Leica). Tissue sections were stained in RNAse-free 0.01% toluidine blue for 2 minutes, dehydrated in xylene 100%, and air dried. Once dry, laser microdissection was done using a laser capture microscope (AS LMD; Leica). The microdissected areas of the tumor were collected in RLT/1% beta-mercaptoethanol solution (RLT-BME; Qiagen).

### RNA extraction and reverse transcription

Total RNA was extracted with the RNEasy Micro Kit (Qiagen) according to manufacturer instructions. RNA quality and quantity were analyzed on a PicoChip (Total Eukaryote RNA Assay Pico II Kit, Qiagen) by capillary electrophoresis (BioAnalyzer; Agilent). Samples with a RNA Integrity Number (RIN) $\geq$7 were considered suitable for qPCR. Then, RNA was retrotranscribed into cDNA using the High Capacity cDNA kit (Applied Biosystems) according to manufacturer instructions.

### Quantitative PCR

Complementary DNA samples were amplified using Low Density Array system according to manufacturer instructions (Applied Biosystems). The arrays were processed on a TaqMan 2900HD (Applied Biosystems). Results were analyzed with the RQ Manager software (Applied Biosystems) and expressed as relative gene expression ($2^{-\Delta\Delta Ct}$ method) using beta-actin expression as endogenous control.

### Statistical analysis

To determine statistical significance of experiments, Wilcoxon rank test and Mann–Whitney test were applied where relevant using the Statview software (SAS Institute). Correlation matrix was done using hierarchical clustering with Genesis software (Institute for Genomics and Bioinformatics, Gratz, Austria; ref. 12). A $P$ value less than 0.05 was considered statistically significant.

## Results

### Ti-BALT T cells are mainly CD4+ memory T cells and most naive T cells home into Ti-BALT

To study the recruitment of T cells into Ti-BALT, we first characterized T-cell subpopulations present in Ti-BALT by confocal microscopy on 15 Ti-BALT from 3 different paraffin-embedded tumors. We observed that Ti-BALT T cells contained both CD4+ and CD8+ T-cell subsets (Fig. 1A), with a clear predominance of CD4+ T cells (88% ± 4% of CD4+ T cells vs. 12% ± 4% of CD8+ T cells; Fig. 1B). On the contrary, CD8+ T cells were largely predominant outside Ti-BALT (data not shown). We then assessed the stage of differentiation of Ti-BALT T cells using CD45RA and CD45RO markers (Fig. 1C and D). We found that most Ti-BALT T cells have a memory phenotype (66% ± 7% of CD45RO+ T cells vs. 34% ± 7% of CD45RA+ naive T cells) (Fig. 1C). However, naive CD45RA+

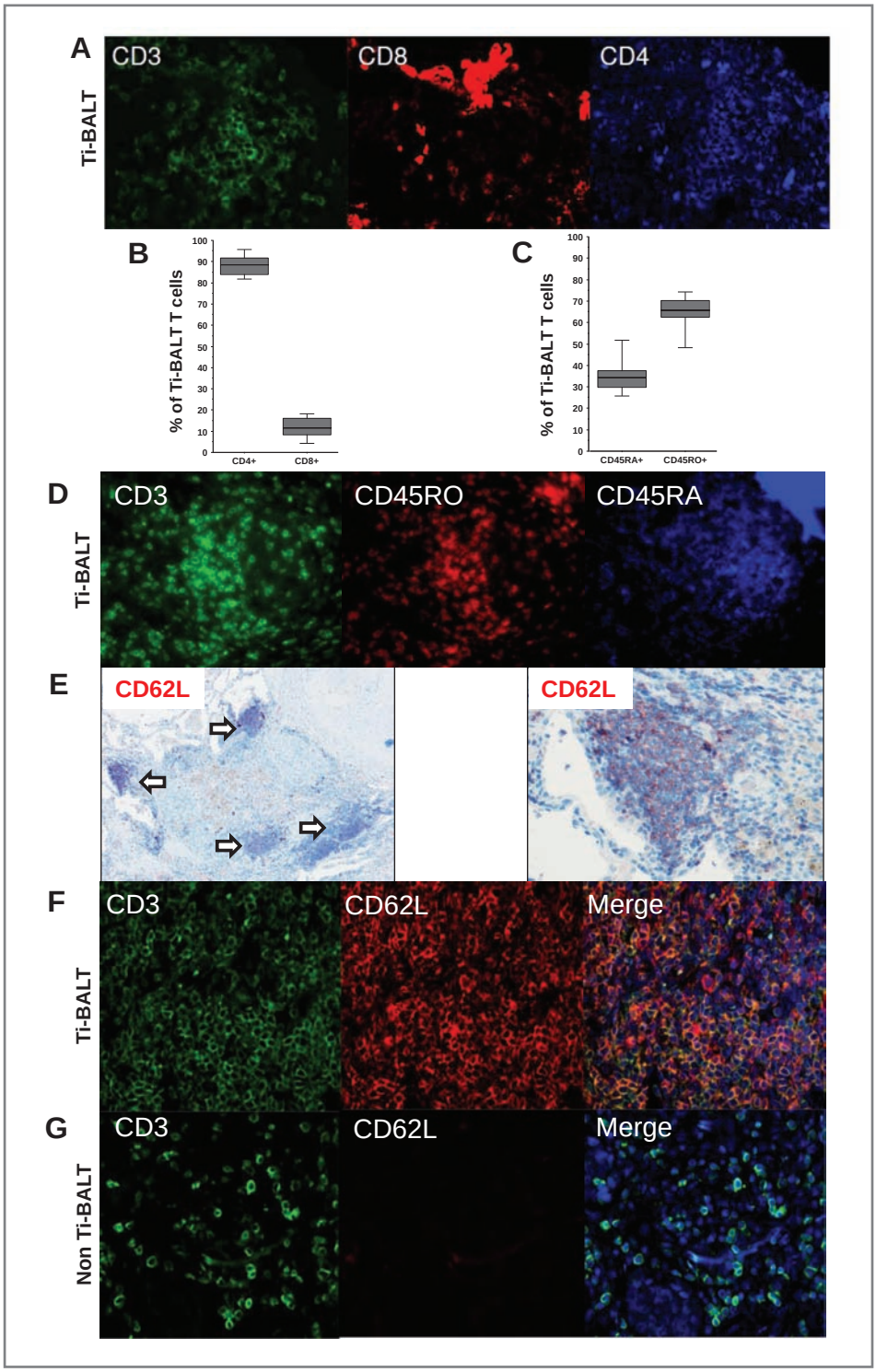


**Figure 1.** Preferential homing of CD4+ and CD45RO+ T cells in Ti-BALT. Multiple immunofluorescent (A, D, F, and G) and immunohistochemistry (E) stainings on paraffin-embedded tumor samples, and quantification (B, C) of T-cell subsets in Ti-BALT ($n = 15$ Ti-BALT from 3 different tumors). Characterization of CD4+ and CD8+ CD3+ T cells (A) as well as CD45RO+ and CD45RA+ CD3+ T cells (D) in Ti-BALT. Selective CD62L expression (red) on Ti-BALT leukocytes (E, left, white arrows) from lung tumor section counterstained by hematoxylin (blue). The right panel represents a higher magnification of the left panel. CD62L+T cells were exclusively detected in Ti-BALT (F) as they were never observed elsewhere in the stroma, or in the tumor nests (G). Original magnification: (A, D), ×250; (E, left), ×100; (E, right panel; F; G), ×400.

T cells were very rarely seen in the other areas of the tumor (data not shown), suggesting that they preferentially localize inside Ti-BALT.

The adhesion molecule CD62L is a lymphoid homing molecule known to be expressed by both naive and central memory T cells. We thus investigated its expression on Ti-BALT T cells by immunohistochemistry and observed that the vast majority of Ti-BALT cells are positive for CD62L (Fig. 1E). In contrast, no CD62L-positive cell could be detected outside the Ti-BALT. To further show these findings, we

showed by confocal microscopy that CD62L is actually expressed on Ti-BALT T cells (Fig. 1F), whereas it is not expressed on T cells located outside these lymphoid structures (Fig. 1G).

Thus, we used CD62L as a Ti-BALT T-cell marker for flow cytometry experiments. Using tumor-infiltrating lymphocytes (TIL) isolated from fresh tumor samples, we confirmed that the main subpopulation of Ti-BALT T cells is CD4+ memory T cells (55% ± 10% of total CD3+ CD62L+ T cells), followed by CD8+ naive T cells (22% ± 10% of CD3+ CD62L+ T cells) and then CD8+ memory T cells and CD4+ naive T cells (11% and 9% of total Ti-BALT T cells, respectively; Fig. 2A).

To determine the predominant localization of the main T-cell subsets in the tumor, we calculated the ratio of CD62L+/total T cells for each subset (Fig. 2B). In line with results described above, we found that Ti-BALT are highly enriched in CD4+ CD45RA+ naive T cells ($n$-fold = 4.3; $P = 0.0009$). The CD4+ CD45RO+ memory T cells ($n$-fold = 1.7; $P = 0.0025$) and the CD8+ CD45RA+ naive T cells ($n$-fold = 2.3; $P = 0.08$) home also preferentially in Ti-BALT ($n$-fold = 1.7; $P = 0.0025$). In contrast, CD8+ CD45RO+ memory T cells were located mainly outside the Ti-BALT ($n$-fold = 3.9; $P = 0.0002$).

Altogether, these data clearly show a selective T-cell distribution within the Ti-BALT with a majority of CD4+ memory T cells and a preferential homing of naive T cells.

### Identification of a chemokine and adhesion molecule signature in Ti-BALT and correlation with CD3 expression

The selective T-cell distribution described above prompted us to investigate the expression of homing molecules associated with Ti-BALT T cell presence. This was done by a laser microdissection approach of both Ti-BALT and tumor nest areas on frozen lung tumor biopsies ($n = 15$; Supplementary Appendix Fig. SA3). The *CD3ε* and *Ep-CAM* genes were used as control markers of Ti-BALT and tumor nest zones, respectively. We compared the gene expression pattern in Ti-BALT versus tumor nests of 66 molecules involved in lymphocyte migration, such as integrins and adhesion molecules (Fig. 3A) and chemoattractants, including all known chemokines (Fig. 3B and C). The relative quantification of these genes normalized to *beta-actin* is presented in Supplementary Appendix Fig. SA4. We then constructed a correlation matrix of gene expression that we submitted to hierarchical clustering (Fig. 3D). This allowed us to determine 2 major clusters of genes displaying similar correlation profile. One cluster contained genes coregulated with *Ep-CAM* (black rectangle) and thus associated with tumor-cell density. The other one contained genes coregulated with CD3ε (red rectangle) and thus associated with T-cell density. We thus identified by differential gene expression, a network of intercorrelated genes associated with T cell presence in Ti-BALT (Table 1), which are likely involved in T-cell recruitment to these lymphoid structures.

### Proteic expression of a set of chemoattractants in Ti-BALT and their counterparts by Ti-BALT T cells

To confirm the potential role of the chemoattractant genes found above, we investigated their proteic expression on

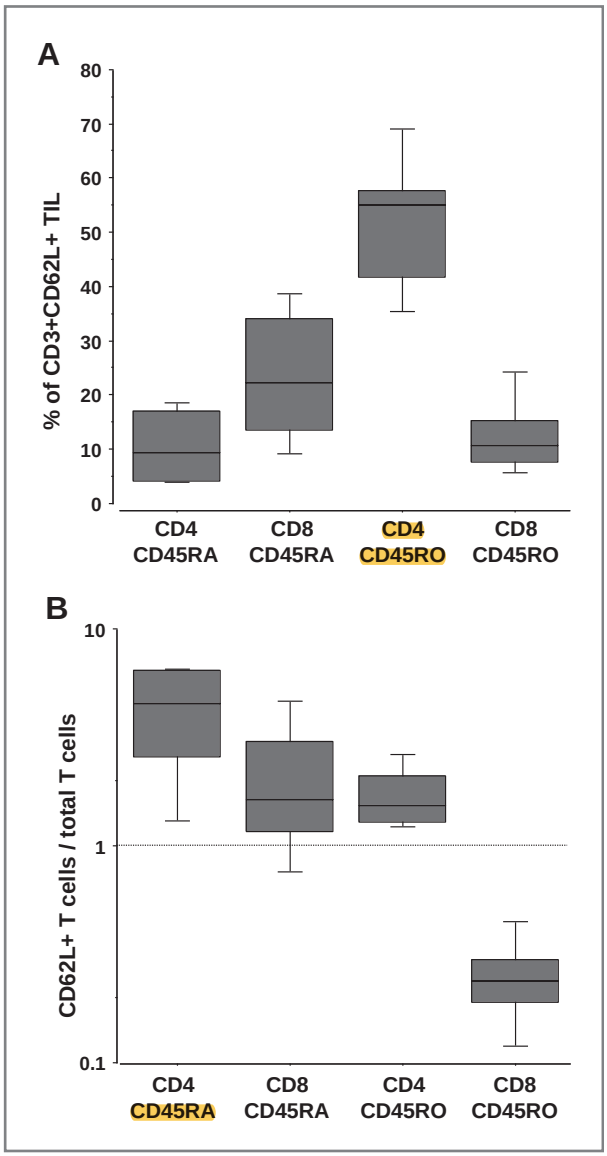


Figure 2. Preferential homing of naive and CD4+ memory T cells in Ti-BALT. Characterization of CD3+ T-cell subpopulations by flow cytometry from fresh lung samples ($n = 10$ tumors). Percentage of CD4+CD45RA+, CD4+CD45R0+, CD8+CD45RA+, and CD8+CD45R0+ among CD3+ CD62L+ TIL (A), and comparison with the percentages of the same populations among total CD3+ TIL (B) by calculating the ratio between these 2 populations.

tumor sections (Fig. 4 and Fig. 5). The lymphoid chemokines CCL19, CCL21, and CXCL13 displayed significant expression in Ti-BALT, whereas they were not expressed in tumor islets (data not shown). The CCL19-positive cells were located in the extrafollicular areas of Ti-BALT (Fig. 4A) and were identified as DC-LAMP+ mature DC (Fig. 5A), whereas CCL21 expression was restricted to lymphatic vessels (Fig. 4B) positive for podoplanin (Fig. 4C and D). CXCL13 was strongly expressed in the germinal centers (Fig. 4E) by CD21+ FDC (Fig. 5B). IL-16 was expressed by most Ti-BALT lymphocytes (Fig. 4F), whereas CCL22 and CCL17 were observed in the Ti-BALT periphery

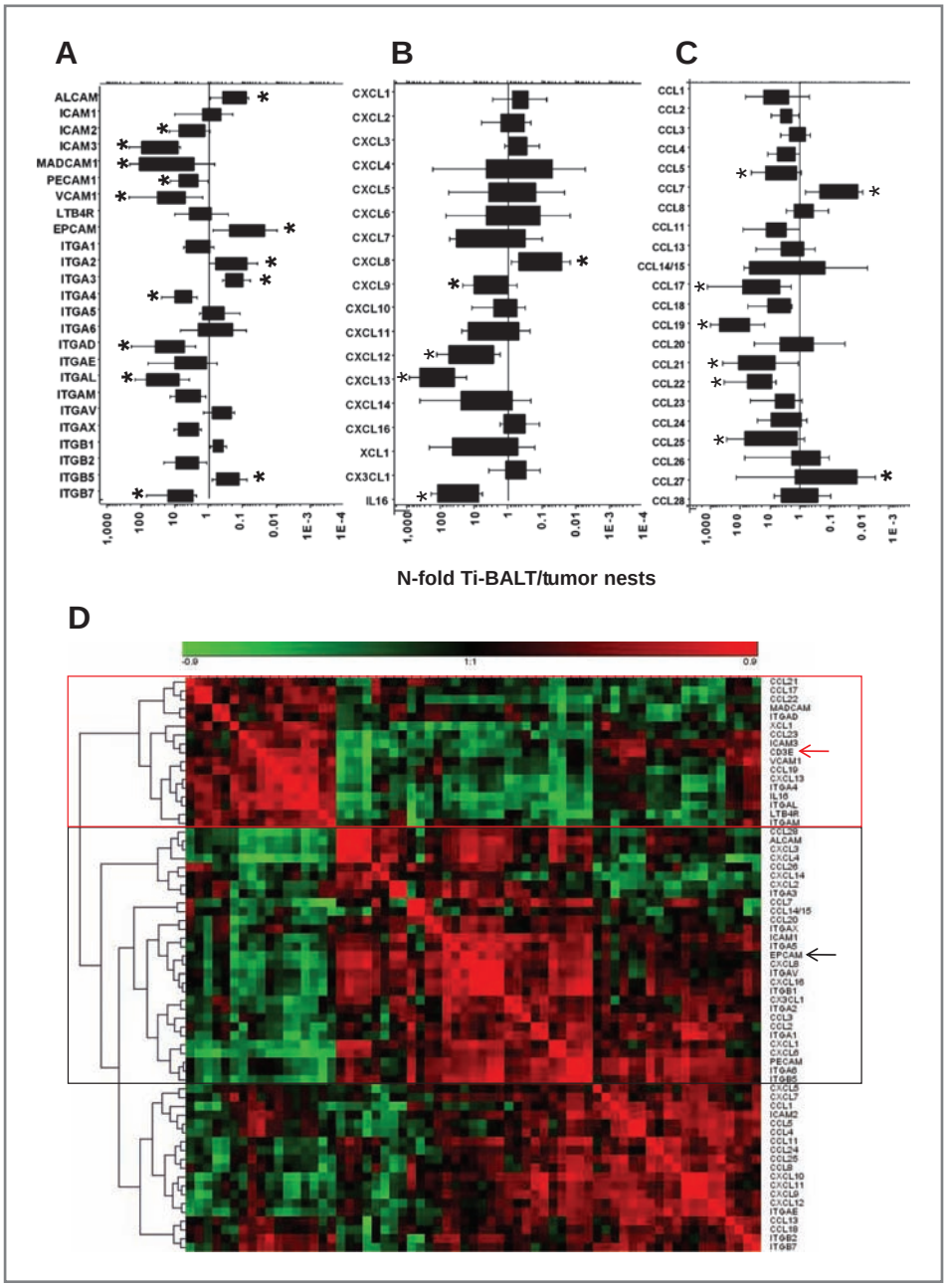


**Figure 3.** Identification of a selective set of genes encoding adhesion molecules and chemoattractants overexpressed in Ti-BALT as compared with tumor nests, and correlating with CD3ε expression. qPCR was done from site-specific total RNA (microdissected Ti-BALT and tumor nests from 15 frozen NSCLC). *Beta-actin* gene was used as housekeeping gene, and *CD3ε* (Ti-BALT) and *Ep-CAM* (tumor nests), as 2 site-control genes. N-fold increase of adhesion molecules and integrins (A), CXC-chemokines and other chemoattractants (B), and CC-chemokines (C) gene expression in Ti-BALT versus tumor nests. Significance of the fold increase was calculated by Wilcoxon rank test: *, $P < 0.05$. A correlation matrix of gene expression in Ti-BALT was constructed and submitted to unsupervised hierarchical clustering using Euclidian distance (D). Each dot represents a correlation coefficient, in which sign is represented by the color of the dot (green for negative correlation, red for positive correlation). The cluster containing *Ep-CAM* gene is delimited by a black border, and the cluster containing *CD3ε* gene is delimited with a red border.

(Fig. 4G and H, respectively) on CD138+ plasma cells (Fig. 5C and D, respectively). These results show that the chemoattractants associated with CD3 expression are actually produced inside the Ti-BALT. We then assessed the expression of all chemokine receptors (CKR) by flow cytometry and confirmed that all receptors of chemokines locally produced are significantly expressed on both CD4+ and CD8+ TIL (Supplementary Appendix Fig. SA5). Furthermore, all chemoattractants receptors associated with T cell presence in Ti-BALT were expressed in a significantly greater proportion of Ti-BALT T cells as compared with non Ti-BALT T cells (Fig. 5E). Altogether, these data provide strong arguments in favor of a role of these chemoattractants in the active recruitment of T-cell subsets to the Ti-BALT.

### HEV colocalize with Ti-BALT and express adhesion molecules strongly associated with T-cell recruitment to Ti-BALT

Having shown that Ti-BALT T cells selectively express CD62L, we investigated whether lung tumors contain HEV, specialized vessels expressing the CD62L ligand PNAd. We found presence of PNAd+ HEV in tumors, exclusively associated with Ti-BALT (Fig. 6A), as they were never observed independently of these lymphoid structures and strictly

**Table 1.** Genes overexpressed in Ti-BALT correlating with CD3 expression

| Family | Gene | N-fold | *P* |
|---|---|---|---|
| Chemoattractants | *CCL19* | 156.91 | <0.0001 |
| | *CXCL13* | 147.61 | <0.0001 |
| | *CCL21* | 31.17 | 0.0002 |
| | *IL16* | 29.10 | <0.0001 |
| | *CCL22* | 13.81 | <0.0001 |
| | *CCL17* | 10.49 | 0.0003 |
| Integrins | *ITGAL* | 20.76 | <0.0001 |
| | *ITGAD* | 10.96 | <0.0001 |
| | *ITGA4* | 4.02 | <0.0001 |
| Adhesion molecules | *ICAM3* | 32.62 | <0.0001 |
| | *VCAM1* | 14.82 | 0.0008 |
| | *MADCAM1* | 11.75 | 0.0019 |
| Control | *CD3ε* | 22.36 | <0.0001 |

NOTE: The table indicates (from left to right): the family of the molecules, name of genes, its fold increase Ti-BALT/tumor nest *(N-fold),* and the *P* value associated with this fold increase (p).

colocalized with CD62L+ cells (Fig. 6B). The HEV seemed functional as red blood cells could readily be seen in the lumen of the venules (Fig. 6B, insert).

To further investigate HEV potential role in lymphocyte recruitment, we analyzed the *in situ* expression of adhesion molecules known to interact with the integrins alpha chains related to T-cell infiltration (alphaL, alphaD, and alpha4; see Table 1). As illustrated in Fig. 6, we observed that $PNAd^+$ HEV were positive for ICAM-2 (Fig. 6C), ICAM-3 (Fig. 6D), VCAM-1 (Fig. 6E), and MAdCAM-1 (Fig. 6F).

Altogether, these data strongly argue for a crucial role of HEV and CD62L/PNAd ligand/receptor pair in lymphocyte recruitment to the Ti-BALT.

## Discussion

A series of lines of evidence suggests that the recruitment of T cells to tumors occurs through intratumoral blood vessels and depends on inflammatory chemokines (13). For the first time, we identified a set of molecules associated with T cells in intratumoral TLS. We also report the presence of PNAd+ HEV specifically associated with the Ti-BALT.

PNAd+ HEV allow the recruitment of both naive and central memory CD62L+ T cells in lymph node (4). Here, we report that CD62L expression is exclusively found on Ti-BALT T cells, whereas PNAd+ HEV were systematically associated with TLS in tumor stroma. This argues strongly that CD62L/PNAd molecules play a similar role in lymphocyte HEV-mediated recruitment in human cancer-associated TLS.

We have also shown the expression of a set of chemoattractants (CCL17, CCL19, CCL21, CCL22, CXCL13, and IL-16) associated with T lymphocytes in Ti-BALT and the expression of their receptors on Ti-BALT-infiltrating T lymphocytes. The

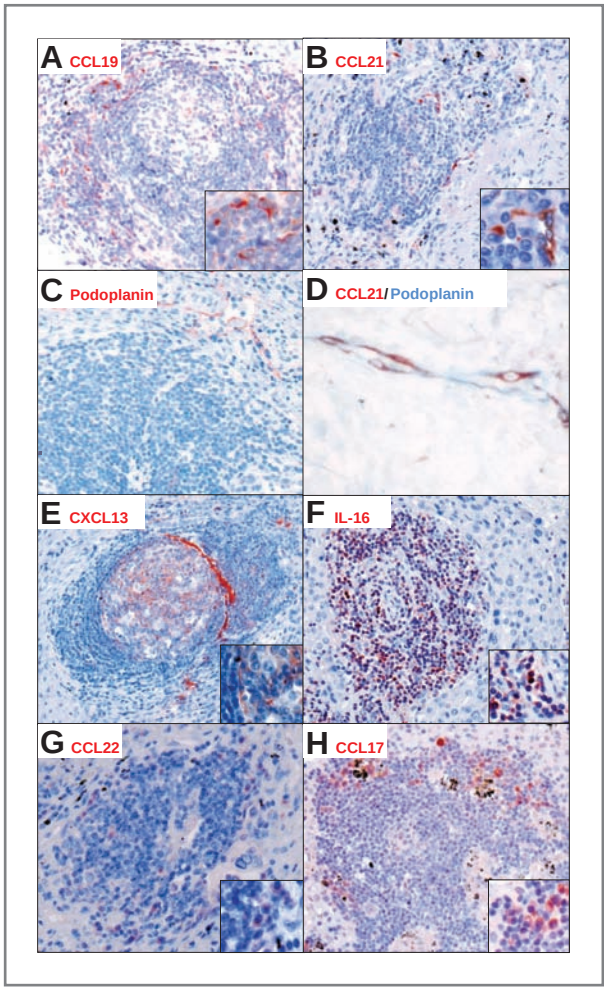


Figure 4. Expression of chemoattractants in Ti-BALT. Single immunostaining followed by hematoxylin counterstaining on paraffin-embedded lung tumor sections. Positive cells (red) for CCL19 (A), CCL21 (B–D), podoplanin (C and D), CXCL13 (E), Il-16 (F), CCL22 (G), and CCL17 (H) were detected in Ti-BALT. Original magnification: ×200. Bottom left inserts show magnification of representative staining patterns.

lymphoid chemokines/receptors CCL19-CCL21/CCR7 and CXCL13/CXCR5 participate in the lymphocyte homing and organization of SLO T-cell zone and B-cell zone, respectively (5). For the first time, we describe the expression of lymphoid chemokines in cancer-associated TLS and their potential role in T lymphocyte recruitment.

Both CCR7 ligands, CCL21 and CCL19, are implicated in the recruitment of activated DC, as well as naive and central memory T-cell subsets to lymph nodes. Interestingly, expression of CCL19 and CCL21 was associated with an increased number of TIL and activated DC in different mouse cancer models (14, 15). These data, together with the fact that CCR7 is expressed by most Ti-BALT T cells, are in line with a role of CCR7 ligands in the recruitment of T cells and, most probably, maturing DC in Ti-BALT. Furthermore, it has recently been shown that DC plays an essential role in pulmonary TLS maintenance (16, 17). Because mature DC in human are known to secrete CCL19 (18), these data suggest that this

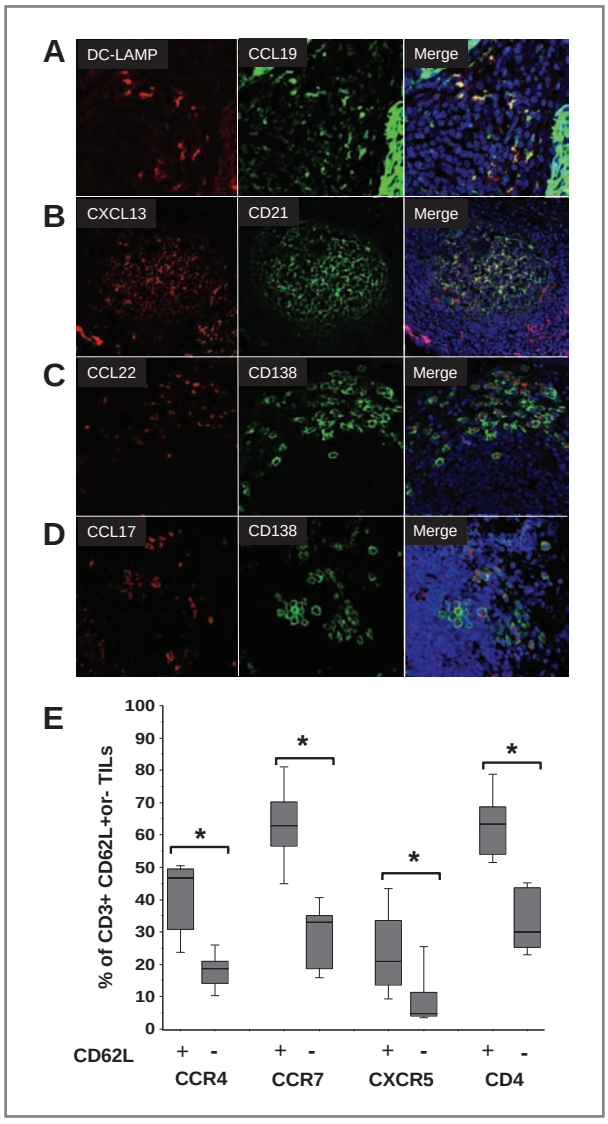


Figure 5. Characterization of cells positives for chemokines and their receptors in Ti-BALT. A–E, double immunofluorescent stainings counterstained with 4′, 6-diamidino-2-phenylindole on paraffin embedded lung tumor sections. Double positive cells for DC-LAMP (activated DC) and CCL19 (A), CD21 (follicular dendritic cells) and CXCL13 (B), CD138 (plasma cells) and CCL22 (C), CD138 and CCL17 (D) were detected in Ti-BALT. Original magnification: (A–D), ×250. E, expression of CCR4, CCR7, CXCR5, and CD4 by flow cytometry on CD3+ TIL recovered from fresh tumor samples ($n = 9$). The expression of CKR was analyzed among CD3+ T cells positive or negative for CD62L molecule. Statistical significance of CKR differential expression between populations was calculated by Mann–Whitney test. *, $P < 0.05$.

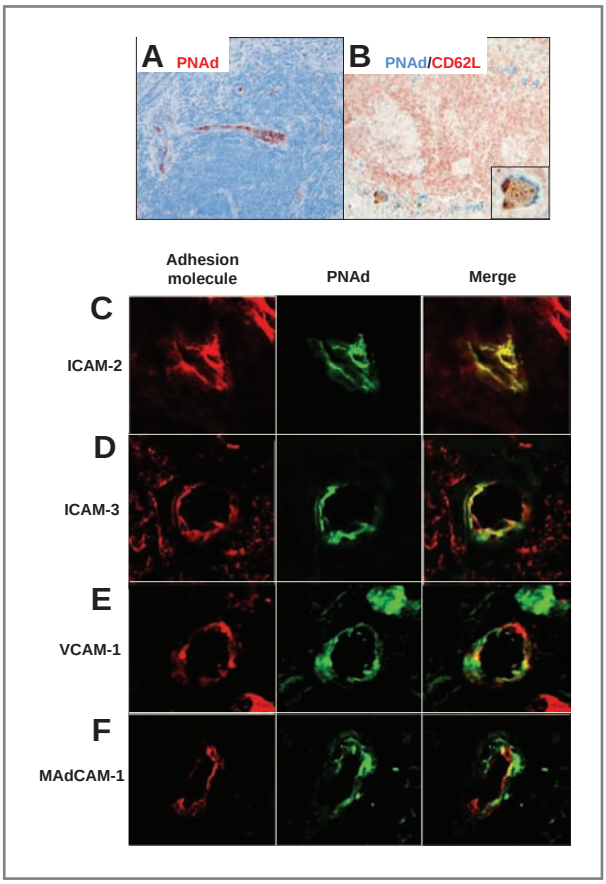


Figure 6. Expression of T-cell–associated adhesion molecules by HEV which selectively colocalize with Ti-BALT. Single (A) and double (B) immunostainings on paraffin-embedded tumor samples. A, presence of PNAd+ HEV (red) in the lung tumor counterstained by hematoxylin. B, colocalization of PNAd+ HEV (blue) with Ti-BALT CD62L+ lymphocytes (red). The bottom right insert show a magnification of a blood vessel containing red blood cells. C–F, double immunofluorescent stainings on frozen lung tumor samples. Expression of the adhesion molecules (red) ICAM2 (C), ICAM3 (D), VCAM-1 (E), and MAdCAM-1 (F) by PNAd+ HEV (green). Original magnification: (A, B), ×200; (C–F), ×400.

cytokine could play a role not only in T-cell recruitment but also in Ti-BALT maintenance.

Expression of CCR4 and its ligands, CCL17 and CCL22, was found in Ti-BALT at the mRNA and protein levels. The CCL17 and CCL22 chemokines have been shown to recruit effector T cells (19–22), as well as regulatory T cells (Treg; refs. 22–25) in cancer mouse models. The ambivalent role of these chemokines is confirmed by the fact that CCL22 has been associated with tumor regression in mouse models (20, 21, 26) and good prognosis in human lung cancer (27), whereas its expression correlates with Treg infiltration and poor prognosis in breast cancer (23). Because many Ti-BALT T cells express CCR4 and Ti-BALT contains very few Treg (data not shown), we hypothesize that this receptor would recruit mostly other T-cell subtypes in these structures.

Finally, the presence of IL-16 has never been reported in cancer or in TLS. Its chemoattractive role for CD4+ T cells and DC is well known (28), and it has been shown to be involved in T-cell recruitment in the pancreas of NOD mice (29). These data as well as the preferential localization of CD4+ T cell and DC populations in the Ti-BALT are good arguments for a direct role of this cytokine in T-cell recruitment in these lymphoid structures.

The association between Ti-BALT and patient survival described previously (6) suggest a role of these structures in antitumoral responses. A possible mechanism sustaining

this effect could be the recruitment of T cells *via* the set of chemoattractants and adhesion molecules described above, followed by the activation and differentiation of effector cells in the Ti-BALT. Interestingly, expression of CCL19 and CCL21 induces tumor regression in different mouse models (14, 15, 30, 31). Moreover, stronger expression of VCAM-1 and MadCAM-1 has been associated to increased survival in colorectal carcinoma (32).

We have found that Ti-BALT T cells consist mainly of memory CD4+ T cells, while being enriched in naive T cells as compared with the rest of the tumor. It has been suggested that CD4+ T cells–DC clusters could recruit naive CD8+ T cells and enhance their activation and differentiation into memory CD8+ T cells in murine lymph nodes (33). More recently, CD4+ T cell help was found to be required for CD8+ T-cell recruitment, activation, and antitumor activity in a mouse model of pancreatic tumors (34). Therefore, we suggest that CD4+ T cells in Ti-BALT recruit naive cells and mature DC and create a favorable microenvironment for T-cell priming by tumor antigen loaded DC. The activated effector cells would then exert a local antitumoral effect, or could act as memory cells.

Indeed, we previously reported the presence of activated DC specifically in Ti-BALT, while Ti-BALT were associated with T-Bet positive Th1 T cells (6). Furthermore, we described a long-term prognostic effect of Ti-BALT density after surgical removal of the tumor, suggesting a role of Ti-BALT in the establishment of a systemic protection involving distant memory cells. At the vicinity of TLS, we found CCL21+ lymphatic vessels (Fig. 4D) which could participate in the emigration of CCR7+ memory Ti-BALT T cells to the draining lymph node. It is not known whether the lymphatic vessels associated with TLS are efferent or afferent, as suggested by Thaunat and colleagues (35). However, the fact that lymphatic vessel density is associated with lymph node invasion in most cancers (36) suggests that at least a part of intratumoral lymphatic vessels can function as efferent. We thus propose that the central memory T cells differentiated in the Ti-BALT could then leave this structure by the associated CCL21+ lymphatic vessels and reach the draining lymph nodes to establish a systemic memory response (Supplementary Appendix Fig. SA6).

Our data argues strongly for a participation of several adhesion molecules and chemokines in T-cell recruitment to intratumoral TLS in NSCLC, some of them being identical to those implied in constitutive lymph node homing. It has been described that T-cell–based immunotherapy regimens suffered from inadequate homing of injected T cells to tumor tissue (37). Therefore, these data could be relevant for designing immunotherapy strategies targeting T cell to the tumor and should be tested accordingly in relevant preclinicals models.

## Disclosure of Potential Conflicts of Interest

No potential conflicts of interest were disclosed.

## Acknowledgments

The authors thank M.C. Klein from the "Centre d'Imagerie Cellulaire et de Cytométrie" (Cordeliers Research Center, Paris) for excellent technical assistance.

## Grant Support

The work was supported by the Institut National de la Santé et de la Recherche Médicale, the Association pour la Recherche sur le Cancer (grant RPT07002DDP) and the Canceropole Ile-de-France (grants RPT09004DDA and R10139DDA).

The costs of publication of this article were defrayed in part by the payment of page charges. This article must therefore be hereby marked *advertisement* in accordance with 18 U.S.C. Section 1734 solely to indicate this fact.

Received March 23, 2011; revised July 19, 2011; accepted August 10, 2011; published OnlineFirst September 7, 2011.

## References

1. Sautès-Fridman C, Cherfils-Vicini J, Damotte D, Fisson S, Fridman WH, Cremer I, et al. Tumor microenvironment is multifaceted. Cancer Metastasis Rev 2011;30:13–25.
2. Pagès F, Galon J, Dieu-Nosjean M, Tartour E, Sautès-Fridman C, Fridman W. Immune infiltration in human tumors: a prognostic factor that should not be ignored. Oncogene 2010;29:1093–102.
3. Ley K, Laudanna C, Cybulsky M, Nourshargh S. Getting to the site of inflammation: the leukocyte adhesion cascade updated. Nat Rev Immunol 2007;7:678–89.
4. Miyasaka M, Tanaka T. Lymphocyte trafficking across high endothelial venules: dogmas and enigmas. Nat Rev Immunol 2004;4:360–70.
5. Cyster JG. Chemokines and cell migration in secondary lymphoid organs. Science 1999;286:2098–102.
6. Dieu-Nosjean M, Antoine M, Danel C, Heudes D, Wislez M, Poulot V, et al. Long-term survival for patients with non-small-cell lung cancer with intratumoral lymphoid structures. J Clin Oncol 2008;26:4410–7.
7. Manzo A, Bombardieri M, Humby F, Pitzalis C. Secondary and ectopic lymphoid tissue responses in rheumatoid arthritis: from inflammation to autoimmunity and tissue damage/remodeling. Immunol Rev 2010;233:267–85.
8. Drayton D, Liao S, Mounzer R, Ruddle N. Lymphoid organ development: from ontogeny to neogenesis. Nat Immunol 2006;7:344–53.
9. Thaunat O, Nicoletti A. Lymphoid neogenesis in chronic rejection. Curr Opin Organ Transplant 2008;13:16–9.
10. Moyron-Quiroz J, Rangel-Moreno J, Hartson L, Kusser K, Tighe M, Klonowski K, et al. Persistence and responsiveness of immunologic memory in the absence of secondary lymphoid organs. Immunity 2006;25:643–54.
11. Moyron-Quiroz J, Rangel-Moreno J, Kusser K, Hartson L, Sprague F, Goodrich S, et al. Role of inducible bronchus associated lymphoid tissue (iBALT) in respiratory immunity. Nat Med 2004;10:927–34.
12. Sturn A, Quackenbush J, Trajanoski Z. Genesis: cluster analysis of microarray data. Bioinformatics 2002;18:207–8.
13. Mantovani A, Savino B, Locati M, Zammataro L, Allavena P, Bonecchi R. The chemokine system in cancer biology and therapy. Cytokine Growth Factor Rev 2010;21:27–39.
14. Hillinger S, Yang S, Batra R, Strieter R, Weder W, Dubinett S, et al. CCL19 reduces tumour burden in a model of advanced lung cancer. Br J Cancer 2006;94:1029–34.
15. Hamanishi J, Mandai M, Matsumura N, Baba T, Yamaguchi K, Fujii S, et al. Activated local immunity by CC chemokine ligand 19-transduced embryonic endothelial progenitor cells suppresses metastasis of murine ovarian cancer. Stem Cells 2010;28:164–73.
16. GeurtsvanKessel C, Willart M, Bergen I, van Rijt L, Muskens F, Elewaut D, et al. Dendritic cells are crucial for maintenance of tertiary lymphoid

structures in the lung of influenza virus-infected mice. J Exp Med 2009;206:2339–49.
17. Halle S, Dujardin H, Bakocevic N, Fleige H, Danzer H, Willenzon S, et al. Induced bronchus-associated lymphoid tissue serves as a general priming site for T cells and is maintained by dendritic cells. J Exp Med 2009;206:2593–601.
18. Kaiser A, Donnadieu E, Abastado JP, Trautmann A, Nardin A. CC chemokine ligand 19 secreted by mature dendritic cells increases naive T cell scanning behavior and their response to rare cognate antigen. J Immunol 2005;175:2349–56.
19. Kanagawa N, Niwa M, Hatanaka Y, Tani Y, Nakagawa S, Fujita T, et al. CC-chemokine ligand 17 gene therapy induces tumor regression through augmentation of tumor-infiltrating immune cells in a murine model of preexisting CT26 colon carcinoma. Int J Cancer 2007;121: 2013–22.
20. Okada N, Sasaki A, Niwa M, Okada Y, Hatanaka Y, Tani Y, et al. Tumor suppressive efficacy through augmentation of tumor-infiltrating immune cells by intratumoral injection of chemokine-expressing adenoviral vector. Cancer Gene Ther 2006;13:393–405.
21. Inoue H, Iga M, Xin M, Asahi S, Nakamura T, Kurita R, et al. TARC and RANTES enhance antitumor immunity induced by the GM-CSF-transduced tumor vaccine in a mouse tumor model. Cancer Immunol Immunother 2008;57:1399–411.
22. Kang S, Xie J, Ma S, Liao W, Zhang J, Luo R. Targeted knock down of CCL22 and CCL17 by siRNA during DC differentiation and maturation affects the recruitment of T subsets. Immunobiology 2010;215: 153–62.
23. Gobert M, Treilleux I, Bendriss-Vermare N, Bachelot T, Goddard-Leon S, Arfi V, et al. Regulatory T cells recruited through CCL22/CCR4 are selectively activated in lymphoid infiltrates surrounding primary breast tumors and lead to an adverse clinical outcome. Cancer Res 2009; 69:2000–9.
24. Qin X, Shi H, Deng J, Liang Q, Jiang J, Ye Z. CCL22 recruits CD4-positive CD25-positive regulatory T cells into malignant pleural effusion. Clin Cancer Res 2009;15:2231–7.
25. Mizukami Y, Kono K, Kawaguchi Y, Akaike H, Kamimura K, Sugai H, et al. CCL17 and CCL22 chemokines within tumor microenvironment are related to accumulation of Foxp3+ regulatory T cells in gastric cancer. Int J Cancer 2008;122:2286–93.
26. Nakazaki Y, Hase H, Inoue H, Beppu Y, Meng X, Sakaguchi G, et al. Serial analysis of gene expression in progressing and regressing mouse tumors implicates the involvement of RANTES and TARC in antitumor immune responses. Mol Ther 2006;14:599–606.
27. Nakanishi T, Imaizumi K, Hasegawa Y, Kawabe T, Hashimoto N, Okamoto M, et al. Expression of macrophage-derived chemokine (MDC)/CCL22 in human lung cancer. Cancer Immunol Immunother 2006;55:1320–9.
28. Kaser A, Dunzendorfer S, Offner F, Ludwiczek O, Enrich B, Koch R, et al. B lymphocyte-derived IL-16 attracts dendritic cells and Th cells. J Immunol 2000;165:2474–80.
29. Meagher C, Beilke J, Arreaza G, Mi QS, Chen W, Salojin K, et al. Neutralization of interleukin-16 protects nonobese diabetic mice from autoimmune type 1 diabetes by a CCL4 dependent mechanism. Diabetes 2010;59:2862–71.
30. Gao J, Sugita T, Kanagawa N, Iida K, Okada N, Mizuguchi H, et al. Anti-tumor responses induced by chemokine CCL19 transfected into an ovarian carcinoma model via fiber-mutant adenovirus vector. Biol Pharm Bull 2005;28:1066–70.
31. Yousefieh N, Hahto S, Stephens A, Ciavarra R. Regulated expression of CCL21 in the prostate tumor microenvironment inhibits tumor growth and metastasis in an orthotopic model of prostate cancer. Cancer Microenviron 2009;2:59–67.
32. Mlecnik B, Tosolini M, Charoentong P, Kirilovsky A, Bindea G, Berger A, et al. Biomolecular network reconstruction identifies T-cell homing factors associated with survival in colorectal cancer. Gastroenterology 2010;138:1429–40.
33. Castellino F, Huang A, Altan-Bonnet G, Stoll S, Scheinecker C, Germain R. Chemokines enhance immunity by guiding naive CD8+ T cells to sites of CD4+ T cell-dendritic cell interaction. Nature 2006;440:890–5.
34. Bos R, Sherman LA. CD4+ T-cell help in the tumor milieu is required for recruitment and cytolytic function of CD8+ T lymphocytes. Cancer Res 2010;70:8368–77.
35. Thaunat O, Kerjaschki D, Nicoletti A. Is defective lymphatic drainage a trigger for lymphoid neogenesis? Trends Immunol 2006;27:441–5.
36. Sleeman J, Thiele W. Tumor metastasis and the lymphatic vasculature. Int J Cancer 2009;125:2747–56.
37. Kapp M, Rasche L, Einsele H, Grigoleit G. Cellular therapy to control tumor progression. Curr Opin Hematol 2009;16:437–43.